scientific reports

Check for updates

OPEN

Dopamine D2 receptor upregulation in dorsal striatum in the *LRRK2*-R1441C rat model of early Parkinson's disease revealed by in vivo PET imaging

Teresa Delgado-Goñi[1,2,9], Natalie Connor-Robson[1,3,9], Milena Cioroch[1,3], Stephen Paisey[4], Christopher Marshall[4], Emma L. Lane[5], David Hauton[6], James McCullagh[6], Peter J. Magill[1,7], Stephanie J. Cragg[1,3], Clare E. Mackay[1,2], Richard Wade-Martins[1,3] & Johannes C. Klein[1,8]✉

We conducted PET imaging with [^{18}F]FDOPA and dopamine D2/3 receptor ligand [^{18}F]fallypride in aged transgenic rats carrying human pathogenic *LRRK2* R1441C or G2019S mutations. These rats have mild age-dependent deficits in dopamine release restricted to dorsal striatum despite no overt loss of dopamine neurons or dopamine content and demonstrate L-DOPA-responsive movement deficits.

***LRRK2* mutant rats displayed no deficit in [^{18}F]FDOPA uptake, consistent with intact dopamine synthesis in striatal axons. However, *LRRK2*-R1441C rats demonstrated greater binding of [^{18}F] fallypride than *LRRK2*-G2019S or non-transgenic controls, from a regionally selective increase in dorsal striatum. Immunocytochemical labelling post-mortem confirmed a greater density of D2 receptors in *LRRK2*-R1441C than other genotypes restricted to dorsal striatum, consistent with upregulation of D2-receptors as a compensatory response to the greater dopamine release deficit previously demonstrated in this genotype.**

These results show that [^{18}F]fallypride PET imaging is sensitive to dysregulation of dopamine signalling in the *LRRK2*-R1441C rat, revealing upregulation of D2 receptors that parallels observations in human putamen in early sporadic PD. Future studies of candidate therapies could exploit this non-invasive approach to assess treatment efficacy.

Keywords [^{18}F]fallypride, [^{18}F]FDOPA, *LRRK2*, Parkinson's disease, PET, Rat

Parkinson's disease (PD) is the second most common human neurodegenerative disease worldwide. It is characterized by progressive dysfunction, degeneration and death of dopaminergic neurons in the substantia nigra pars compacta (SNc), which project to the dorsal striatum. Striatal dopamine deficiency is the core deficit underlying the main motor problems of the disease[1,2]. PD is also a multi-system disorder with behavioural, cognitive, and autonomic features, which can precede motor disease by decades[3]. When motor symptoms establish a PD diagnosis, patients have already lost about 60–80% of their dopaminergic neurons[4,5].

The mechanisms of PD pathogenesis are incompletely understood, hindering the development of neuroprotective therapies[4]. Genetic factors are thought to contribute to perhaps 10% of PD cases[6]. In recent years, new transgenic animal models have been developed based on known PD-associated genes[7–11] and are aiding discovery of mechanisms contributing to disease progression from early prodromal stages through to late neurodegeneration, as well as providing new models for identifying biomarkers and testing treatments. Several

[1]Oxford Parkinson's Disease Centre (OPDC), University of Oxford, Oxford, UK. [2]Department of Psychiatry, University of Oxford, Oxford, UK. [3]Department of Physiology, Anatomy and Genetics, University of Oxford, Oxford, UK. [4]Wales Research and Diagnostic PET Imaging Centre (PETIC), School of Medicine, Heath Park, Cardiff University, Cardiff, Wales, UK. [5]School of Pharmacy and Pharmaceutical Sciences, Cardiff University, Cardiff, Wales, UK. [6]Department of Chemistry, University of Oxford, Oxford, UK. [7]Medical Research Council Brain Network Dynamics Unit, University of Oxford, Oxford, UK. [8]Wellcome Centre for Integrative Neuroimaging, FMRIB, Nuffield Department of Clinical Neurosciences, University of Oxford, Oxford, UK. [9]Teresa Delgado-Goñi and Natalie Connor-Robson contributed equally to this work. ✉email: johannes.klein@ndcn.ox.ac.uk

rodent models have been developed based on mutations in the leucine-rich repeat kinase 2 gene (*LRRK2).* LRRK2 mutations are the most common cause of dominantly inherited PD[12] and account for around 1% of sporadic PD[13]. The G2019S mutation is the most frequent[14] but, the R1441C mutation induces a more aggressive phenotype[15]. LRRK2 rodent models reproduce age-dependent and progressive motor and cognitive impairment of PD[10,16–19].

We have previously generated and described Bacterial Artificial Chromosome (BAC) *LRRK2* transgenic rats, expressing either *LRRK2*-R1441C or *LRRK2*-G2019S forms of the human *LRRK2* genomic locus[10,20,21]. These rats exhibit mild age-dependent impairments in dopamine release in dorsal but not ventral striatum, in the absence of any loss of dopaminergic markers (tyrosine hydroxylase [TH], vesicular monoamine transporter 2 [VMAT2] or dopamine transporter [DAT]) in the striatum[10,20], but paralleled by more dispersed synaptic vesicles and reduced phosphorylated synapsin[20]. In addition, *LRRK2*-R1441C rats display age-dependent reductions in burst firing of dopamine neurons in SNc and have L-DOPA-responsive motor dysfunction. In young adult rats (3–6 mon old), there were no differences in the firing rate or regularity of SNc dopamine neurons between either *LRRK2*-R1441C or *LRRK2*-G2019S and non-transgenic controls. However, in aged rats of both genotypes (16–22 mon old), SNc dopamine neurons showed a significant decrease in firing variability compared to controls, with firing patterns becoming more regular. Young adult LRRK2-G2019S rats (3–6 mon) showed enhanced performance on the rotarod test compared to non-transgenic controls. In contrast, aged G2019S rats (18–21 mon) exhibited significant impairment on the rotarod test compared to both non-transgenic and human wild-type *LRRK2* controls. Similarly, aged (18–21 mon) LRRK2-R1441C rats showed impaired motor performance on the rotarod test compared to controls, while young (3–6 months) *LRRK2*-R1441C rats did not exhibit motor impairment. The motor deficits in aged rats of both genotypes were reversed by L-DOPA treatment, linking the age-dependent changes in dopamine neuron function summarised above to the observed motor symptoms[10].

However, no SNc neurodegeneration or abnormal protein accumulation is detectable in these models, suggesting that they represent an early stage of PD and that nigrostriatal dopaminergic dysfunction can precede detectable pathology in early stages of the disease[10]. In conclusion, the histopathology in this animal model is distinct to early manifest human PD, where many presynaptic neurons are lost before motor symptoms arise. Toxin-based models, like the 6-OHDA rodent model[22,23], generate significant presynaptic neuronal loss in a short space of time using non-transgenic animals. Genetic models, like the LRRK2 model used here, require more time and investment to generate, but have distinct physiological advantages over the toxin-based models[24]. They allow for a more gradual, progressive development of PD-like pathology and PD symptoms appearing later in life, like how the human disease progresses, and indeed share the genetic origin of familial human PD. This way, they also maintain compensatory neuroplasticity that can occur in early PD stages. In contrast, toxin-based models cause rapid, acute and less specific damage. Moreover, genetic models affect multiple brain regions and systems, not just the nigrostriatal pathway targeted by lesions. Lastly, the progressive nature allows testing of interventions to slow/prevent neurodegeneration, and there is great potential for imaging biomarkers quantifying disease in determining efficacy of these interventions.

Neuroimaging techniques offer a non-invasive strategy to assess dopaminergic dysfunction early in disease, to monitor disease progression, and to assess experimental therapeutic strategies in PD animal models before translation to humans[25]. However, there is little available data to indicate whether PET studies can reveal modifications to nigrostriatal function in new generation, physiological transgenic models of early stages of PD, prior to overt degeneration. PET imaging studies in humans during onset of DA degeneration reveal reductions in dopaminergic presynaptic markers and increased binding of dopamine D2-receptor ligands[26,27]. Moreover, increased D2-receptor binding in early PD can be localized to the putamen rather than caudate or ventral striatum, and is thought to be an adaptive increase in postsynaptic D2-receptor levels in response to declining levels of dopamine release, rather than due to lower competition for receptor binding from lower levels of endogenous dopamine[26,27]. Increased striatal D2-ligand binding has also been seen in PET imaging in toxin-based animal models of PD, in 6-OHDA rats[28,29], and MPTP-exposed monkeys[30] but has not yet been explored or validated in more physiological models of nigrostriatal dysfunction prior to degeneration. One study to date has assessed presynaptic function in *LRRK2*-G2019S rats at 12 months but did not detect significant changes[31].

Several PET tracers are suitable for imaging dopaminergic function in rodents. The tracer 6-[^{18}F]fluoro-L-DOPA ([^{18}F]FDOPA) is a marker of pre-synaptic dopamine synthesis capacity, and [^{18}F]fallypride indicates dopamine D2/D3 receptor levels[32,33]. We assessed whether PET imaging of [^{18}F]FDOPA and [^{18}F]fallypride could identify changes to respectively presynaptic function or dopamine receptor levels, using the Waxholm atlas (Fig. 1A), and compared susceptible dorsal versus spared ventral striatum (Fig. 1B), in *LRRK2*-R1441C and *LRRK2*-G2019S transgenic rat models of early PD, and assessed corresponding D2-receptor immunolabelling (Table 1).

Results

Dopamine synthesis capacity is preserved in LRRK2-G2019S and LRRK2-R1441C genotypes

Specific [^{18}F]FDOPA uptake was detected in the striatum, with an acceptable CNR of 3.5 ± 0.93 (Fig. 2A). Figure 2B shows an example Patlak plot obtained from the striatum. No significant differences were detected in [^{18}F]FDOPA uptake between left and right striata (Table S1). Average uptake data from both striata (Table 2, Fig. 2C) indicate that animals carrying either the *LRRK2*-G2019S or the *LRRK2*-R1441C mutation showed no significant deficit in [^{18}F]FDOPA uptake in comparison to nTG animals.

D2/D3 receptor binding is upregulated in the dorsal striatum in aged LRRK2-R1441C rats

D2/D3-receptor ligand [^{18}F]fallypride PET imaging of resulted in a striatal CNR of 19.6 ± 3.88, giving clear delineation of the rat striatum compared to background (Fig. 3A). Delayed acquisition Logan Reference Plots of

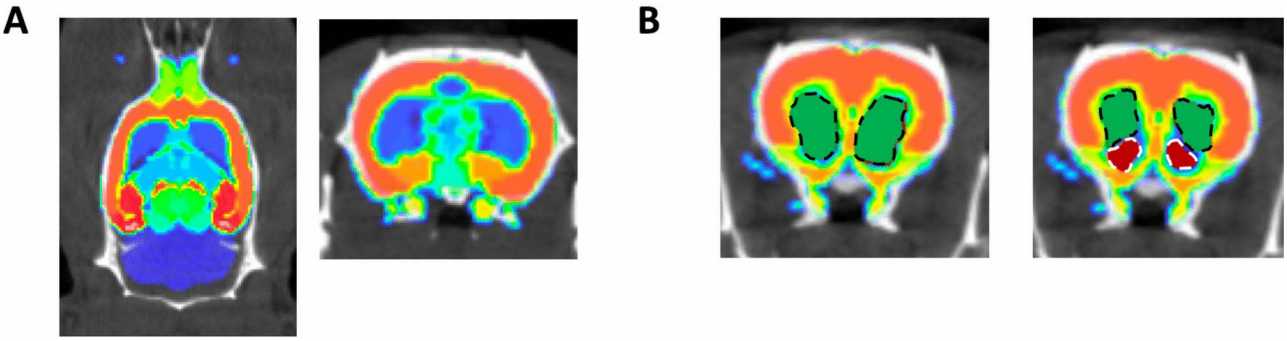

Fig. 1. Colour-coded rat brain region templates. (**A**) Waxholm rat brain template from[61,62] superimposed to a representative CT scan from one of the LRRK2 rats included in the PET study. Arbitrary colours to distinguish atlas regions. Left, axial orientation; Right, coronal. (**B**) Left, Coronal images showing ROIs calculated using the connected threshold tool and the rat brain template covering left and right striatum (green areas delimited by a black discontinuous line). Right, ROIs calculated for dorsal (green areas delimited by a black discontinuous line) and ventral striatum (red areas delimited by white discontinuous lines).

	[^{18}F]FDOPA		[^{18}F] Fallypride		IHC
	Female	Male	Female	Male	
nTG	7	4	4	1	3
G2019S	5	5	2	3	3
R1441C	8	7	6	5	3
Total	36		21		9

Table 1. Summary of animal numbers in the study. Numbers of rats by sex, genotype and tracer.

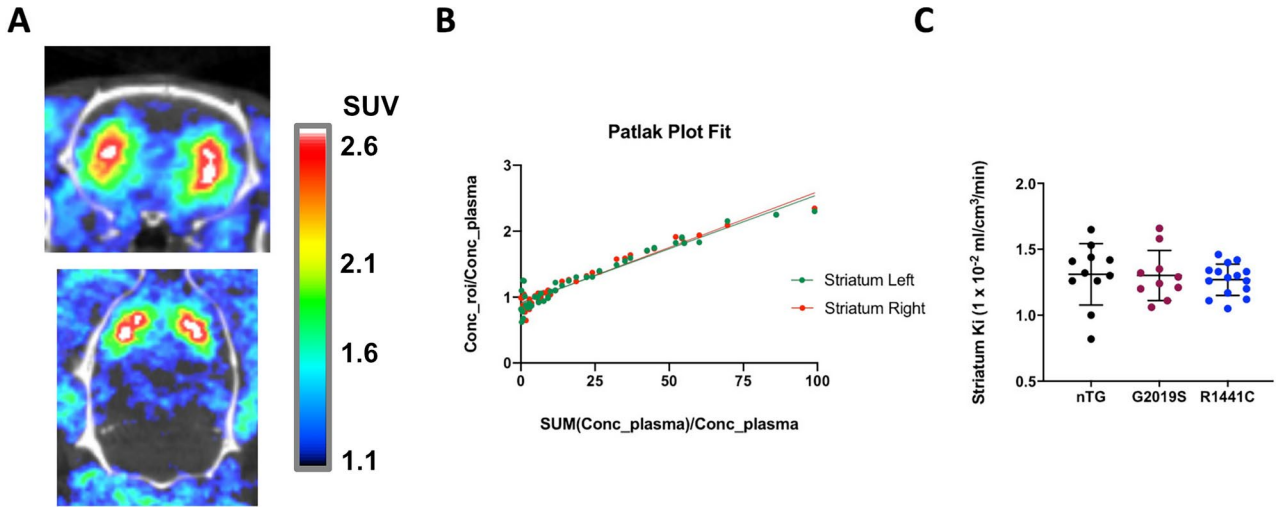

Fig. 2. [^{18}F]FDOPA PET imaging. (**A**) Representative [^{18}F]FDOPA PET images acquired in the same animal from coronal (top) and axial (bottom) orientations. The BQML scale range shows the 95% and the 40% of the maximum signal detected as maximum and minimum values respectively. (**B**) Patlak plot modelling applied to a representative animal to assess [^{18}F]FDOPA dynamic uptake in left and right striatum. (**C**) Striatal [^{18}F] FDOPA Ki compared between nTG, *LRRK2*-G2019S and *LRRK2*-R1441C genotypes using a One-way ANOVA test followed by pot-hoc comparisons (Tukey HSD). Each dot on the plot represents data from a single rat. * $p < 0.05$.

	[18F]FDOPA Ki (×10^{-2} ml/cm^3/min)	[18F]fallypride DVR		
		Total striatum	Dorsal	Ventral
nTG	1.31 ± 0.23	15.99 ± 4.05	15.92 ± 3.96§	9.96 ± 1.92
G2019S	1.30 ± 0.19	16.28 ± 3.15	15.97 ± 2.53§	9.73 ± 0.76
R1441C	1.27 ± 0.12	20.93 ± 2.19*	21.21 ± 2.46§§**	10.55 ± 1.16

Table 2. [18F]FDOPA and [18F]fallypride PET tracer dynamic uptake. Average dynamic tracer uptake in the striatum of animals in the 3 groups investigated. [18F]fallypride DVR in dorsal and ventral striatal segmentations is also shown. Data represent mean ± SD. One- or Two-way ANOVA tests followed by post-hoc comparisons (Tukey HSD) were used to compare between genotypes (*$p < 0.05$; **$p < 0.01$) and between regions within genotype: $^{\S}p < 0.01$; $^{\S\S}p < 0.001$.

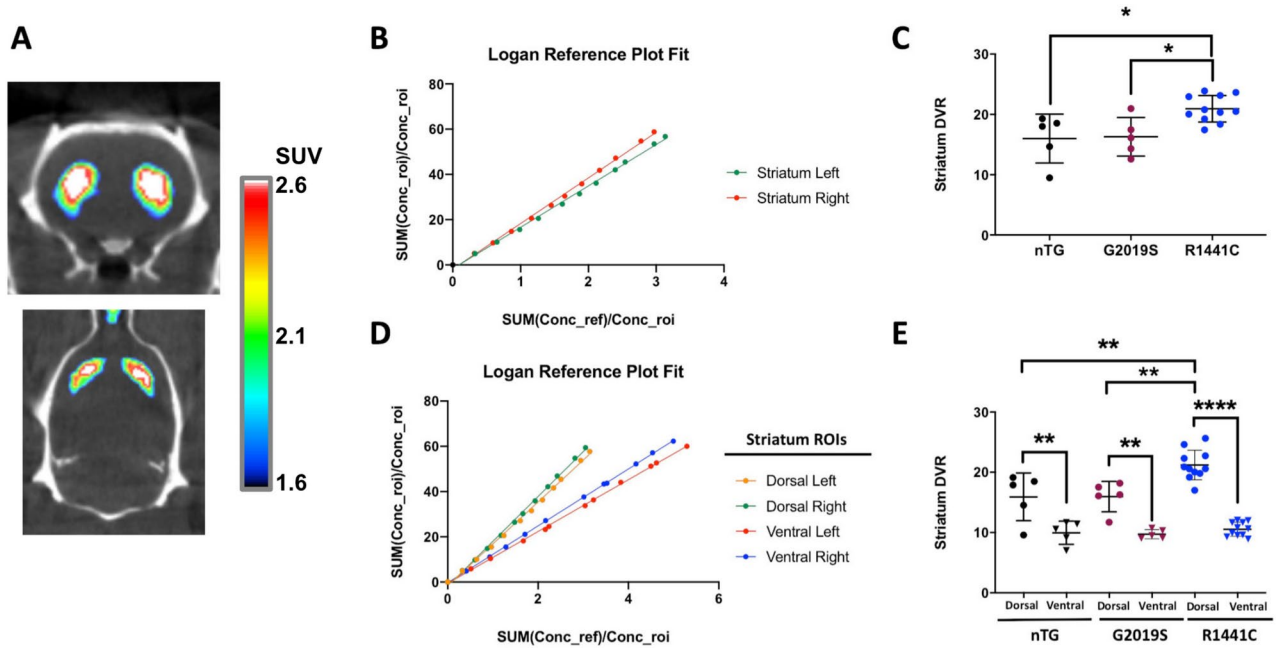

Fig. 3. [18F]fallypride PET imaging reveals elevated levels in dorsal striatum of *LRRK2*-R1441C rats. (**A**) Representative [18F]fallypride PET images acquired in the same animal from coronal (top) and axial (bottom) orientations. The BQML scale range shows the 95% and the 40% of the maximum signal detected as maximum and minimum values respectively. (**B**) Logan Reference plot modelling applied to the representative case to assess [18F]fallypride dynamic uptake in left and right striatum (One-way ANOVA and Tukey). (**C**) Striatal [18F]fallypride DVR compared between nTG, *LRRK2*-G2019S and *LRRK2*-R1441C groups. D and E show the same analysis approach described in B and C but segmenting the striatum in dorsal and ventral regions Two-way ANOVA for genotype and region, post-hoc Tukey tests: *$p < 0.05$; **$p < 0.01$; ****$p < 0.0001$.

tracer binding in an example animal are shown in Fig. 3B. No tracer uptake difference was found between left and right striata (Table S3).

The level of whole striatal [18F]fallypride varied with genotype (One-Way ANOVA, $F_{2,18} = 0.422$, $p = 0.006$), with *LRRK2-R1441C* rats showing significantly higher binding compared to nTG and *LRRK2-G2019S* groups (Table 2, Fig. 3C; post-hoc Tukey tests, $p = 0.015$ and $p = 0.023$ respectively). Comparison of the ventral and dorsal subdivisions of striatum, revealed significant differences between genotypes and regions, and a significant interaction (Two-way ANOVA, $F_{2,36} = 5.50$, $p = 0.008$). There was a significant difference between dorsal and ventral striatal [18F]fallypride binding (Two-way ANOVA, $F_{1,36} = 106.9$, $p < 0.001$), owing to greater [18F]fallypride binding in dorsal striatum compared to ventral striatum in each of the three genotypes investigated (nTG, $p = 0.002$; G2019S, $p = 0.002$ and R1441C, $p < 0.001$) (Table 2, Fig. 3D,E). Furthermore, the significant effect of genotype ($F_{2,36} = 9.38$, $p = 0.001$), resulted from [18F]fallypride binding within the dorsal striatum of *LRRK2*-R1441C rats being significantly greater than in nTG ($p = 0.001$) and *LRRK2*-G2019S ($p = 0.001$) rats. There was no difference in [18F]fallypride binding between genotypes for the ventral striatum.

D2 receptor immunoreactivity is elevated in dorsal striatum in LRRK2-R1441C rats

[18F]fallypride binds D2 and D3 receptors, but D3 receptor levels are very low in the striatum in comparison to those of D1 and D2 receptors[34]. To identify whether [18F]fallypride binding corresponded to D2-receptor

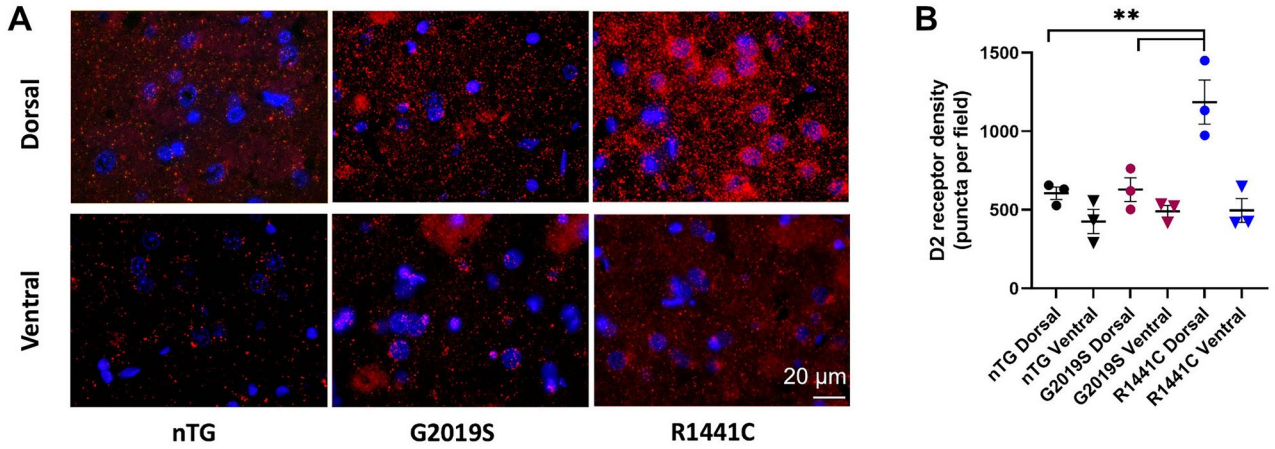

Fig. 4. D2-receptor density is elevated in dorsal striatum of *LRRK2*-R1441C rats. (**A**) D2 receptors visualised with immunofluorescence staining. Scale bar 20 µm. (**B**) Quantification of D2-receptor density, n = 3 per genotype. Data represent mean ± SEM. Post-hoc Tukey tests, for clarity, only comparisons between genotypes for dorsal striatum are indicated $^{**}p < 0.01$.

levels, D2 receptor expression in the 3 genotypes (nTG, *LRRK2*-G2019S and *LRRK2*-R1441C) was assessed using indirect immunofluorescence (Fig. 4A) in dorsal and ventral striatum. There were significant differences in density of immunolabelling between genotypes and regions, and a significant interaction (Two-way ANOVA, $F_{2,12} = 7.08$, $p = 0.009$). There was a significant difference between dorsal and ventral striatal immunolabelling (Two-way ANOVA, $F_{1,12} = 25.38$, $p < 0.001$), owing to greater D2-receptor density in dorsal striatum compared to ventral striatum in *LRRK2*-R1441C rats only (Tukey post-hoc test, $p = 0.001$). The significant effect of genotype ($F_{2,12} = 9.38$, $p = 0.004$) was due to greater D2-receptor levels in dorsal striatum of *LRRK2*-R1441C rats than in any other region of any other genotype (Fig. 4B).

Discussion

We used non-invasive PET imaging to test the utility of the imaging technique for assessing nigrostriatal dysfunction in early-stage PD models of wild-type and mutant human LRRK2-expressing rats. [^{18}F]fallypride imaging identified upregulation of dopamine receptor binding in the dorsal striatum of LRRK2-R1441C transgenic rats, which corresponded to the upregulation of D2-receptor density identified with immunolabeling. Dysregulation of dopamine release and dopamine neuron physiology had previously been identified in this model[10], and we speculate that relative dopamine depletion at the post-synaptic neuron drives upregulation of D2 receptor density. This is similar to observations in a lesional macaque model[35], a lesional rodent model[36], and to PET studies in early human PD[26,27,37]. Another group found upregulation of striatal D2 receptors in an alpha-synuclein overexpressing PD rat model[38], suggesting that this feature is shared with our chosen model of PD.

LRRK2 BAC transgenic rats have been characterised in several measures of presynaptic and behavioural function[10,20,21]. Both G2019S and R1441C mutations induce dysregulation of the endocytic pathway and changes in the distribution of synaptic vesicles in dopaminergic neurons. Animals carrying either mutation develop motor and cognitive impairments at an advanced age and display deficits in evoked dopamine release in dorsal striatum, but not in ventral striatum, compared to nTG rats. Dopamine release deficits are greater in *LRRK2*-R1441C than *LRRK2*-G2019S rats. In addition, *LRRK2*-R1441C rats only show a lower frequency of bursts and a lower percentage of spikes fired in bursts compared to nTG rats, as well as a more severe disease phenotype[10]. However, post-synaptic dopamine receptor levels and function had not previously been assessed in these models.

[^{18}F]fallypride is a high affinity and highly selective dopamine D2/D3 receptor ligand with negligible affinity for other neuroreceptors[39], giving it favourable characteristics for imaging dopamine receptor levels in this PD rat model. Its performance has been characterised in rodents[40,41], including toxin-induced models of PD[29], but not previously in transgenic models of early PD. We found greater dopamine receptor binding in the *LRRK2-R1441C* genotype than in the other genotypes, which was regionally selective to the dorsal striatum. The dopamine receptor upregulation found in *LRRK2*-R1441C rats is complementary to the impairments in evoked dopamine release we saw previously in this model[10]: These impairments, as measured by sub-second fast scan cyclic voltammetry, are observed in the dorsal, but not the ventral striatum in *LRRK2* mutant aged rats, with a more severe deficit in *LRRK2*-R1441C than *LRRK2*-G2019S rats. Dopamine receptor upregulation in the *LRRK2*-R1441C rat dorsal striatum is consistent with early human PD where, similar to our data, an increase in dopamine receptor density is seen in the putamen, but not the caudate nucleus[26]. In human PD, initial upregulation of dopamine receptors is thought to be a post-synaptic response to dopamine input loss. It is reversed in advanced PD, where a decrease of dopamine receptor density is seen[42–44]. Dopamine receptor upregulation is a candidate compensation mechanism that allows the human motor system to function until the striate dopamine depletion is advanced[45,46]. Now, it also provides a readout of early dopaminergic dysfunction, and we have shown that this can be detected by [^{18}F]fallypride PET in the *LRRK2*-R1441C model.

Differences in dopamine receptor tracer binding can reflect dopamine receptor availability[29] resulting from either lower dopamine occupancy from low release levels[47,48], or from greater receptor levels[49] or both. We validated here that differences in [^{18}F]fallypride binding between regions and genotypes reflected differences in the density of the D2 receptor. The greater [^{18}F]fallypride binding and D2-receptor levels in *LRRK2*-R1441C compared to *LRRK2*-G2019S rats is consistent with greater upregulation of post-synaptic D2 receptors arising from the more severe impairment in dopamine release seen in the *LRRK2*-R1441C rat. The more severe phenotype seen with the R1441C rather than the G2019S mutation might in part arise from the fact that these mutations reside in different enzymatic domains of the *LRRK2* gene (the GTPase versus kinase domains respectively), and therefore exert differing effects on the enzymatic activity of *LRRK2*, and consequentially, differing impact on cellular function[21]. It cannot arise from simple concentration differences, as the expression of mutant LRRK2 in the G2019S genotype is greater than in the R1441C model[10].

The *LRRK2* BAC transgenic models selected for this study exhibit age-dependent and L-DOPA responsive motor dysfunction. In the absence of widespread cell death in this model[10], the L-DOPA-rescuable PD phenotype suggests that axonal (synaptic) dysfunction precedes overt degeneration of the dopaminergic neurons[50], causing functional dopamine "deprivation" of postsynaptic neurons. PD animal models capturing α-synuclein pathology have also reported early changes in striatal dopamine release without concomitant differences in striatal dopamine content[8,51], supporting the hypothesis that synaptic dysfunction precede overt neurodegeneration. Our findings here reveal that the synaptic adaptations occurring without frank dopamine neuron degeneration extend to an upregulation in striatal dopamine receptor density in dorsal striatum, that can be detected with a non-invasive approach of PET imaging.

This study has limitations, including the relatively small sample size. Secondly, the ex-vivo histology and in-vivo PET imaging were performed on different animal cohorts, which prevents direct correlation between imaging and histological findings in the same animals. However this approach guards against chance findings by providing complementary evidence from separate modalities and separate animal cohorts. Western blotting could have provided a more quantitative approach to the measurement of D2 receptor expression, although separating the small sub-regions of the caudateputamen for analysis is challenging. Finally, isoflurane anaesthesia during PET scanning may influence tracer binding. Anaesthetics generally affect cerebral blood flow, and isoflurane may also reduce endogenous dopamine release[52].

In conclusion, [^{18}F]fallypride PET imaging is sensitive to early dopaminergic dysfunction in the striatum in the LRRK2-R1441C rat model of PD. This non-invasive approach could be used in the future to assess efficacy of new candidate therapies longitudinally in the model.

Material and methods

Animals

LRRK2 BAC transgenic rats on a Sprague–Dawley background were generated and genotyped as previously reported[10]. Forty-five aged animals (age 21–22 mon) including both males and females (weight 350–945 g) were used in this study: non-transgenic rats (nTG, n = 11 for PET plus 3 for histology), and two mutant lines, expressing either the *LRRK2*-G2019S (n = 10 plus 3) or *LRRK2*-R1441C (n = 15 plus 3) mutant forms of the human gene (Table 1). Rat weights did not differ between genotypes (Body weight nTG 550 ± 152 g, G2019S 640 ± 169 g, R1441C 573 ± 142 g; Kruskal–Wallis $p = 0.79$).

All experiments were conducted in accordance with the Animals (Scientific Procedures) Act, 1986 (United Kingdom) and the University of Oxford Policy on the Use of Animals in Scientific Research, and the ARRIVE guidelines[53]. As previously described, LRRK2-expressing BAC transgenic rats were housed with littermate controls[10]. Rats were housed in a 12 h light–dark cycle with ad-libitum access to food and water. Both sexes were used throughout this study. Rats were humanely euthanised using carbon dioxide inhalation in a purpose-designed chamber, following approved institutional procedures for rodent euthanasia.

PET acquisition

PET molecular imaging studies were carried out on isoflurane-anaesthetised rats using a Mediso 122S nanoScan PET/CT scanner using an integral multicell XXL rat bed (Mediso Medical Imaging Systems, Budapest, Hungary). 36 animals were scanned with [^{18}F]FDOPA, and after complete ^{18}F decay, 21 of them underwent an additional scan with [^{18}F]fallypride on a different day. [^{18}F]FDOPA and [^{18}F]fallypride were produced in house at the Wales Research and Diagnostic PET Imaging Centre (PETIC) on a Trasis all-in-one system. [^{18}F]fallypride synthesis was performed based on the method described by Mukherjee et al., using nucleophilic fluorination of the tosyl precursor followed by HPLC purification and reformulation[54]. [^{18}F]FDOPA synthesis was performed with high specific activity via a nucleophilic route from ^{18}F-fluoride in a multistep procedure[55].

We used the high-throughput delayed [^{18}F]fallypride imaging protocols developed by Tantawy et al[56], which allows more animals to be scanned per tracer synthesis. Onset of scanning was one hour after [^{18}F]fallypride injection. PET data were acquired in list mode into a 128 × 128 × 95-matrix. The coincidence window width was set at 6 nsec. PET images were reconstructed with the scanner manufacturer's nucline software (400 µm resolution, CT based attenuation correction, Tera-tomo 3D reconstruction algorithm, using a full detector model, 4 iterations and 6 subsets). At the end of the PET scan, a 3 min CT was acquired (50 kVp, 360 rotations) for anatomical localisation and attenuation correction.

General anaesthetic was delivered through a nose cone and maintained during the scanning protocol (2–2.5% isoflurane/100% oxygen, 1.5 L/min). Temperature was maintained at 37 °C via hot air flow through the bed, and breathing was monitored via a pneumatic sensing pad (~ 60 breaths/min). The tail vein was cannulated 15 min before scanning using a 22G/25 mm cannula (Millpledge MP06222, UK) attached to an Anisite membrane locking cap (Millpledge HB07510, UK).

For [^{18}F]FDOPA experiments, animals were injected i.p. with the COMT inhibitor entacapone (40 mg/kg, Glentham Life Sciences GP9755, UK) in a DMSO/saline solution (60/40 v/v, 11.85 mg/ml) adjusted to pH 7 with NaOH solution (1 M, 1–10 µL), 90 min before tracer administration. The peripheral Aromatic L-Amino Acid Decarboxylase (AADC) inhibitor benserazide hydrochloride (10 mg/kg, Glentham Life Sciences GP7664, UK) was administered in aqueous solution (10 mg/ml), 60 min before tracer injection[57]. Benserazide does not cross the blood–brain barrier. This inhibitor combination is licensed for oral use in PD patients receiving L-DOPA treatment[58], and ensures that L-DOPA (and here, [^{18}F]FDOPA) reaches the brain intact.

[^{18}F]FDOPA was injected as a single bolus (nTG 148 ± 14.2 MBq/kg, G2019S 148 ± 25 MBq/kg, R1441C 152 ± 15.8 MBq/kg) followed by saline flush (50 µL). A 90 min single bed position PET scan was acquired in 3D list mode starting immediately at the end of radiotracer injection[59]. The raw PET data were sorted into 41 frame-dynamic sinograms as follows: 6 × 10 s, 6 × 30 s, 11 × 60 s, 15 × 180 s, 3 × 600 s.

[^{18}F]fallypride scans were carried out with the same scanner set-up and animal preparation used for [^{18}F]DOPA, with the exception that no inhibitors are required before tracer injection. [^{18}F]fallypride dose was injected at nTG 72 ± 2.8 MBq/kg, G2019S 70 ± 12.4 MBq/kg, R1441C 72 ± 8.1 MBq/kg; followed by a saline flush (50 µL). Anaesthesia of the rat was maintained outside the scanner for a 60 min uptake period before a 60 min PET scan was acquired in 3D list mode starting at the delayed timepoint of 60 min post radiotracer injection. Data were sorted into 12 × 300 s timeframes[56].

Tracer cold masses injected and specific activities at injection are shown in Tables S2 and S4 in the supplementary material.

Molecular imaging analysis

PET images were analysed using VivoQuant® software with an additional pharmacokinetic modelling module (Vivoquant 4.0 patch 3, Invicro, Boston, MA, US). Regions of interest (ROIs) corresponding to left and right striatum were extracted from the Waxholm atlas and applied to individual scans. A representative cerebellum region consisting of a 60 mm^3 sphere placed in the centre of the cerebellum was drawn with the free hand tool, to provide a reference input function for tracer uptake analysis.

Data were processed using two different approaches: (i) dynamic analysis of tracer uptake during the full scanning time with multiple-time graphical analysis (Patlak and Logan plots as appropriate), and, for comparison, (ii) calculation of tracer uptake from static imaging (standardized uptake value (SUV)) derived from the last 30 min of acquisition. Static images were also used to calculate contrast-to-noise (CNR) for both tracers.

[^{18}F]FDOPA data were analysed with Patlak plots, analogous to previous approaches[59]. The 10 initial minutes from each scan were discarded for analysis purposes[60]. Left and right target striatal ROI influx estimates (Ki) were averaged and used for group-wise analysis.

[^{18}F]fallypride PET imaging was used to assess D2/D3 receptor levels in the striatum of nTG, *LRRK2*-G2019S and *LRRK2*-R1441C animals. Logan reference plots over the entire 60-min scan period were applied to [^{18}F]fallypride data with the cerebellum used as a reference region. Note that the [^{18}F]fallypride scans were acquired at 60 to 120 min post tracer injection, thus a t* of 0 min used in software equates to a real-world t* of 60 min. Left and right ROI distribution volume ratio (DVR) values were averaged for each rat and subjected to statistical analysis. The high CNR of [^{18}F]fallypride scans allowed further subdivision of the rat striatum into dorsal and ventral sections (Fig. 1B). This was not possible in the case of [^{18}F]FDOPA as the initially lower CNR was severely decreased after region segmentation, affecting Patlak plot fitting (Supplementary Material, Figure S1). The Waxholm atlas[61,62] was used in combination with VivoQuant® software for ROI delineation and [^{18}F]fallypride DVR was calculated in these sub-regions as described above. The anatomic distribution of the ROIs used in the segmented analysis is shown in Figure S2.

Immunolabeling

An additional rat cohort (n = 9) was used for the immunofluorescence validation of D2 receptor expression levels. Animals were culled under terminal anaesthesia using pentobarbital (0.7 g/kg, i.p.) and transcardially perfused with 0.01 M phosphate buffered saline (pH 7.4) followed by 4% w/v paraformaldehyde in 0.01 M phosphate buffered saline. Paraffin embedded brain sections, cut to a thickness of 8 µm, were dewaxed and rehydrated through a series of alcohol. Slides were blocked in PBS-Tween (0.4% v/v tween) containing 10% v/v normal donkey serum for 60 min at room temperature, then incubated with the primary D2 receptor antibody (ab85367, Abcam, UK) (1:250 dilution in PBS-Tween with 10% normal donkey serum) over night at 4 °C. Samples were then washed and incubated with the secondary antibody (A-21207, ThermoFisher) (1:1000 dilution in PBS-Tween) for 1 h at room temperature, thereafter, washed and incubated in 1 µg/ml DAPI (Life Technologies). Coverslips were mounted onto Superfrost plus (VWR) microscope slides using FluorSave reagent (Millipore). Samples were imaged using an Invitrogen EVOSTM FL Auto cell imaging system at 60 × magnification. Eight images were acquired in the dorsal and 6 in the ventral striatum for each animal. D2 receptor staining was quantified with the ImageJ software (v1.52n, NIH, USA) using the particle analysis module after applying background subtraction (rolling:35) and the unsharp masking filter (radius:1; mask weight:0.8).

Statistical analysis

Statistical analyses were performed using SPSS 23 (IBM, USA) and GraphPad Prism 8 and 9 (GraphPad Software, USA). Data were analysed by One- or Two-way analysis of variance (ANOVA), or Student's t-tests. In instances when group size did not allow for standard tests of normality (i.e. Shapiro–Wilk, Kolmogorov–Smirnov), the normality of the residuals was assessed instead. Post-hoc tests following ANOVAs were conducted using Tukey HSD correction. Two-tailed levels of significance were used and $p < 0.05$ was considered statistically significant. Data are expressed as mean ± standard deviation (SD) throughout the manuscript.

Data availability

All data needed to evaluate the conclusions in this manuscript are present in the manuscript and/or the Supplementary Materials.

Received: 14 August 2023; Accepted: 21 April 2025
Published online: 07 May 2025

References

1. Poewe, W. et al. Parkinson disease. *Nat. Rev. Dis. Primers* **3**, 17013. https://doi.org/10.1038/nrdp.2017.13 (2017).
2. Politis, M. Neuroimaging in Parkinson disease: From research setting to clinical practice. *Nat. Rev. Neurol.* **10**, 708–722. https://doi.org/10.1038/nrneurol.2014.205 (2014).
3. McGregor, M. M. & Nelson, A. B. Circuit mechanisms of Parkinson's disease. *Neuron* **101**, 1042–1056. https://doi.org/10.1016/j.neuron.2019.03.004 (2019).
4. Dauer, W. & Przedborski, S. Parkinson's disease: Mechanisms and models. *Neuron* **39**, 889–909. https://doi.org/10.1016/s0896-6273(03)00568-3 (2003).
5. Kordower, J. H. et al. Disease duration and the integrity of the nigrostriatal system in Parkinson's disease. *Brain* **136**, 2419–2431. https://doi.org/10.1093/brain/awt192 (2013).
6. Tysnes, O. B. & Storstein, A. Epidemiology of Parkinson's disease. *J. Neural Transm. (Vienna)* **124**, 901–905. https://doi.org/10.1007/s00702-017-1686-y (2017).
7. Vingill, S., Connor-Robson, N. & Wade-Martins, R. Are rodent models of Parkinson's disease behaving as they should?. *Behav. Brain Res.* **352**, 133–141. https://doi.org/10.1016/j.bbr.2017.10.021 (2018).
8. Janezic, S. et al. Deficits in dopaminergic transmission precede neuron loss and dysfunction in a new Parkinson model. *Proc. Natl. Acad. Sci. U S A* **110**, E4016-4025. https://doi.org/10.1073/pnas.1309143110 (2013).
9. Ninkina, N. et al. A novel resource for studying function and dysfunction of alpha-synuclein: Mouse lines for modulation of endogenous Snca gene expression. *Sci. Rep.* **5**, 16615. https://doi.org/10.1038/srep16615 (2015).
10. Sloan, M. et al. LRRK2 BAC transgenic rats develop progressive, L-DOPA-responsive motor impairment, and deficits in dopamine circuit function. *Hum. Mol. Genet.* **25**, 951–963. https://doi.org/10.1093/hmg/ddv628 (2016).
11. Yue, M. et al. Progressive dopaminergic alterations and mitochondrial abnormalities in LRRK2 G2019S knock-in mice. *Neurobiol. Dis.* **78**, 172–195. https://doi.org/10.1016/j.nbd.2015.02.031 (2015).
12. Spatola, M. & Wider, C. Genetics of Parkinson's disease: The yield. *Parkinsonism Relat. Disord.* **20**(Suppl 1), S35-38. https://doi.org/10.1016/S1353-8020(13)70011-7 (2014).
13. Baig, F. et al. Delineating nonmotor symptoms in early Parkinson's disease and first-degree relatives. *Mov. Disord.* **30**, 1759–1766. https://doi.org/10.1002/mds.26281 (2015).
14. Li, J. Q., Tan, L. & Yu, J. T. The role of the LRRK2 gene in Parkinsonism. *Mol. Neurodegener.* **9**, 47. https://doi.org/10.1186/1750-1326-9-47 (2014).
15. Criscuolo, C. et al. The LRRK2 R1441C mutation is more frequent than G2019S in Parkinson's disease patients from southern Italy. *Mov. Disord.* **26**, 1733–1736. https://doi.org/10.1002/mds.23735 (2011).
16. Breger, L. S. & Fuzzati Armentero, M. T. Genetically engineered animal models of Parkinson's disease: From worm to rodent. *Eur. J. Neurosci.* **49**, 533–560. https://doi.org/10.1111/ejn.14300 (2019).
17. Creed, R. B. & Goldberg, M. S. New developments in genetic rat models of Parkinson's disease. *Mov. Disord.* **33**, 717–729. https://doi.org/10.1002/mds.27296 (2018).
18. Volta, M. & Melrose, H. LRRK2 mouse models: dissecting the behavior, striatal neurochemistry and neurophysiology of PD pathogenesis. *Biochem. Soc. Trans.* **45**, 113–122. https://doi.org/10.1042/BST20160238 (2017).
19. Xiong, Y. et al. Robust kinase- and age-dependent dopaminergic and norepinephrine neurodegeneration in LRRK2 G2019S transgenic mice. *Proc. Natl. Acad. Sci. U S A* **115**, 1635–1640. https://doi.org/10.1073/pnas.1712648115 (2018).
20. Connor-Robson, N. et al. An integrated transcriptomics and proteomics analysis reveals functional endocytic dysregulation caused by mutations in LRRK2. *Neurobiol. Dis.* **127**, 512–526. https://doi.org/10.1016/j.nbd.2019.04.005 (2019).
21. Wallings, R., Connor-Robson, N. & Wade-Martins, R. LRRK2 interacts with the vacuolar-type H+-ATPase pump a1 subunit to regulate lysosomal function. *Hum. Mol. Genet.* **28**, 2696–2710. https://doi.org/10.1093/hmg/ddz088 (2019).
22. Nikolaus, S., Antke, C. & Müller, H. W. In vivo imaging of synaptic function in the central nervous system. *Behav. Brain Res.* **204**(1), 1–31. https://doi.org/10.1016/j.bbr.2009.06.008 (2009).
23. Nikolaus, S. et al. In vivo imaging neurotransmitter function: The rat 6-hydroxydopamine model and its relevance for human Parkinson's disease. *Nuklearmedizin* **50**(04), 155–156. https://doi.org/10.3413/Nukmed-0371-10-12 (2011).
24. Dawson, T. M., Ko, H. S. & Dawson, V. L. Genetic animal models of Parkinson's disease. *Neuron* **66**, 646–661. https://doi.org/10.1016/j.neuron.2010.04.034 (2010).
25. Strome, E. M. & Doudet, D. J. Animal models of neurodegenerative disease: insights from in vivo imaging studies. *Mol. Imaging Biol.* **9**, 186–195. https://doi.org/10.1007/s11307-007-0093-4 (2007).
26. Kaasinen, V. et al. Upregulation of putaminal dopamine D2 receptors in early Parkinson's disease: A comparative PET study with [11C] raclopride and [11C]N-methylspiperone. *J. Nucl. Med.* **41**, 65–70 (2000).
27. Rinne, J. O. et al. Increased density of dopamine D2 receptors in the putamen, but not in the caudate nucleus in early Parkinson's disease: A PET study with [11C]raclopride. *J. Neurol. Sci.* **132**, 156–161. https://doi.org/10.1016/0022-510x(95)00137-q (1995).
28. Creese, I., Burt, D. R. & Snyder, S. H. Dopamine receptor binding enhancement accompanies lesion-induced behavioral supersensitivity. *Science* **197**, 596–598. https://doi.org/10.1126/science.877576 (1977).
29. Mann, T. et al. [18F]fallypride-PET/CT analysis of the dopamine D2/D3 receptor in the hemiparkinsonian rat brain following intrastriatal botulinum neurotoxin a injection. *Molecules* **23**(3), 587. https://doi.org/10.3390/molecules23030587 (2018).
30. Leenders, K. L. et al. Unilateral MPTP lesion in a rhesus monkey: effects on the striatal dopaminergic system measured in vivo with PET using various novel tracers. *Brain Res.* **445**, 61–67. https://doi.org/10.1016/0006-8993(88)91074-8 (1988).
31. Walker, M. D. et al. Behavioral deficits and striatal DA signaling in LRRK2 p.G2019S transgenic rats: a multimodal investigation including PET neuroimaging. *J. Parkinson's Disease* **4**(3), 483–498. https://doi.org/10.3233/JPD-140344 (2014).
32. Loane, C. & Politis, M. Positron emission tomography neuroimaging in Parkinson's disease. *Am. J. Transl. Res.* **3**, 323–341 (2011).
33. Vuckovic, M. G. et al. Exercise elevates dopamine D2 receptor in a mouse model of Parkinson's disease: In vivo imaging with [(1)(8)F]fallypride. *Mov. Disord.* **25**, 2777–2784. https://doi.org/10.1002/mds.23407 (2010).
34. Araki, K. Y., Sims, J. R. & Bhide, P. G. Dopamine receptor mRNA and protein expression in the mouse corpus striatum and cerebral cortex during pre- and postnatal development. *Brain Res.* **1156**, 31–45. https://doi.org/10.1016/j.brainres.2007.04.043 (2007).
35. Bezard, E. et al. Relationship between the appearance of symptoms and the level of nigrostriatal degeneration in a progressive 1-methyl-4-phenyl-1,2,3,6-tetrahydropyridine-lesioned macaque model of Parkinson's disease. *J. Neurosci.* **21**, 6853–6861. https://doi.org/10.1523/JNEUROSCI.21-17-06853.2001 (2001).
36. Hume, S. P. et al. Effect of L-dopa and 6-hydroxydopamine lesioning on [11C]raclopride binding in rat striatum, quantified using PET. *Synapse* **21**, 45–53. https://doi.org/10.1002/syn.890210107 (1995).

37. Rinne, J. O. et al. PET study on striatal dopamine D2 receptor changes during the progression of early Parkinson's disease. *Mov. Disord* **8**, 134–138. https://doi.org/10.1002/mds.870080203 (1993).
38. Stokholm, K. et al. α-Synuclein overexpression increases dopamine D2/3 receptor binding and immune activation in a model of early Parkinson's disease. *Biomedicines* **9**, 1876. https://doi.org/10.3390/biomedicines9121876 (2021).
39. Grunder, G. et al. Brain and plasma pharmacokinetics of aripiprazole in patients with schizophrenia: An [18F]fallypride PET study. *Am. J. Psychiatry* **165**, 988–995. https://doi.org/10.1176/appi.ajp.2008.07101574 (2008).
40. Constantinescu, C. C., Coleman, R. A., Pan, M. L. & Mukherjee, J. Striatal and extrastriatal microPET imaging of D2/D3 dopamine receptors in rat brain with [(1)(8)F]fallypride and [(1)(8)F]desmethoxyfallypride. *Synapse* **65**, 778–787. https://doi.org/10.1002/syn.20904 (2011).
41. Mukherjee, J. et al. Dopamine D3 receptor binding of (18)F-fallypride: Evaluation using in vitro and in vivo PET imaging studies. *Synapse* **69**, 577–591. https://doi.org/10.1002/syn.21867 (2015).
42. Niccolini, F., Su, P. & Politis, M. Dopamine receptor mapping with PET imaging in Parkinson's disease. *J. Neurol.* **261**, 2251–2263. https://doi.org/10.1007/s00415-014-7302-2 (2014).
43. Rinne, J. O., Laihinen, A., Lonnberg, P., Marjamaki, P. & Rinne, U. K. A post-mortem study on striatal dopamine receptors in Parkinson's disease. *Brain Res.* **556**, 117–122. https://doi.org/10.1016/0006-8993(91)90554-9 (1991).
44. Zaja-Milatovic, S. et al. Dendritic degeneration in neostriatal medium spiny neurons in Parkinson disease. *Neurology* **64**, 545–547. https://doi.org/10.1212/01.WNL.0000150591.33787.A4 (2005).
45. Bezard, E., Gross, C. E. & Brotchie, J. M. Presymptomatic compensation in Parkinson's disease is not dopamine-mediated. *Trends Neurosci.* **26**, 215–221. https://doi.org/10.1016/S0166-2236(03)00038-9 (2003).
46. Blesa, J. et al. Compensatory mechanisms in Parkinson's disease: Circuits adaptations and role in disease modification. *Exp. Neurol.* **298**, 148–161. https://doi.org/10.1016/j.expneurol.2017.10.002 (2017).
47. Goggi, J. L. et al. Dopamine transporter neuroimaging accurately assesses the maturation of dopamine neurons in a preclinical model of Parkinson's disease. *Stem Cell Res. Ther.* **11**, 347. https://doi.org/10.1186/s13287-020-01868-4 (2020).
48. Ota, M., Ogawa, S., Kato, K., Masuda, C. & Kunugi, H. Striatal and extrastriatal dopamine release in the common marmoset brain measured by positron emission tomography and [(18)F]fallypride. *Neurosci. Res.* **101**, 1–5. https://doi.org/10.1016/j.neures.2015.07.008 (2015).
49. Christian, B. T., Narayanan, T. K., Shi, B. & Mukherjee, J. Quantitation of striatal and extrastriatal D-2 dopamine receptors using PET imaging of [(18)F]fallypride in nonhuman primates. *Synapse* **38**, 71–79. https://doi.org/10.1002/1098-2396(200010)38:1%3c71::AID-SYN8%3e3.0.CO;2-2 (2000).
50. Burke, R. E. & O'Malley, K. Axon degeneration in Parkinson's disease. *Exp. Neurol.* **246**, 72–83. https://doi.org/10.1016/j.expneurol.2012.01.011 (2013).
51. Lundblad, M., Decressac, M., Mattsson, B. & Bjorklund, A. Impaired neurotransmission caused by overexpression of alpha-synuclein in nigral dopamine neurons. *Proc. Natl. Acad. Sci. U S A* **109**, 3213–3219. https://doi.org/10.1073/pnas.1200575109 (2012).
52. Opacka-Juffry, J., Ahier, R. G. & Cremer, J. E. Nomifensine-induced increase in extracellular striatal dopamine is enhanced by isoflurane anaesthesia. *Synapse* **7**, 169–171. https://doi.org/10.1002/syn.890070210 (1991).
53. Kilkenny, C., Browne, W. J., Cuthill, I. C., Emerson, M. & Altman, D. G. Improving bioscience research reporting: The ARRIVE guidelines for reporting animal research. *PLoS Biol.* **8**, e1000412. https://doi.org/10.1371/journal.pbio.1000412 (2010).
54. Mukherjee, J., Yang, Z. Y., Das, M. K. & Brown, T. Fluorinated benzamide neuroleptics—III. Development of (S)-N-[(1-allyl-2-pyrrolidinyl)methyl]-5-(3-[18F]fluoropropyl)-2,3-dimethoxybenzamide as an improved dopamine D-2 receptor tracer. *Nuclear Med. Biol.* **22**(3), 283–296. https://doi.org/10.1016/0969-8051(94)00117-3 (1995).
55. Kuik, W. J. et al. In vivo biodistribution of no-carrier-added 6–18F-fluoro-3,4-dihydroxy-L-phenylalanine (18F-DOPA), produced by a new nucleophilic substitution approach, compared with carrier-added 18F-DOPA, prepared by conventional electrophilic substitution. *J. Nucl. Med.* **56**, 106–112. https://doi.org/10.2967/jnumed.114.145730 (2015).
56. Tantawy, M. N. et al. [(18)F]Fallypride dopamine D2 receptor studies using delayed microPET scans and a modified Logan plot. *Nucl. Med. Biol.* **36**, 931–940. https://doi.org/10.1016/j.nucmedbio.2009.06.007 (2009).
57. Walker, M. D. et al. Measuring dopaminergic function in the 6-OHDA-lesioned rat: A comparison of PET and microdialysis. *EJNMMI Res.* **3**, 69. https://doi.org/10.1186/2191-219X-3-69 (2013).
58. Eggert, K. et al. Direct switch from levodopa/benserazide or levodopa/carbidopa to levodopa/carbidopa/entacapone in Parkinson's disease patients with wearing-off: efficacy, safety and feasibility–an open-label, 6-week study. *J. Neural Trans. (Vienna)* **117**, 333–342. https://doi.org/10.1007/s00702-009-0344-4 (2010).
59. Kyono, K. et al. Use of [18F]FDOPA-PET for in vivo evaluation of dopaminergic dysfunction in unilaterally 6-OHDA-lesioned rats. *EJNMMI Res.* **1**, 25. https://doi.org/10.1186/2191-219X-1-25 (2011).
60. Becker, G. et al. Comparative assessment of 6-[(18) F]fluoro-L-m-tyrosine and 6-[(18) F]fluoro-L-dopa to evaluate dopaminergic presynaptic integrity in a Parkinson's disease rat model. *J. Neurochem.* **141**, 626–635. https://doi.org/10.1111/jnc.14016 (2017).
61. Osen, K. K., Imad, J., Wennberg, A. E., Papp, E. A. & Leergaard, T. B. Waxholm Space atlas of the rat brain auditory system: Three-dimensional delineations based on structural and diffusion tensor magnetic resonance imaging. *Neuroimage* **199**, 38–56. https://doi.org/10.1016/j.neuroimage.2019.05.016 (2019).
62. Papp, E. A., Leergaard, T. B., Calabrese, E., Johnson, G. A. & Bjaalie, J. G. Waxholm space atlas of the sprague dawley rat brain. *Neuroimage* **97**, 374–386. https://doi.org/10.1016/j.neuroimage.2014.04.001 (2014).

Acknowledgements

This work was supported by the Oxford Parkinson's Disease Centre, funded by the Monument Trust Discovery Award from Parkinson's UK (Grant J-1403), with the support of the National Institute for Health Research (NIHR) Biomedical Research Centres based at Oxford University Hospitals NHS Trust, Oxford Health NHS Foundation Trust and University of Oxford, and the NIHR Clinical Research Network. Dr Klein acknowledges support from the National Institute for Health and Care Research (NIHR) Oxford Health Clinical Research Facility, and the NIHR Oxford Biomedical Research Centre (BRC). P.J.M. was supported by the Medical Research Council UK (award MC_UU_12024/2). The Wellcome Centre for Integrative Neuroimaging is supported by core funding from the Wellcome Trust (203139/Z/16/Z and 203139/A/16/Z).

Author contributions

J.C.K., C.E.M., R.W-M, T.D-G., N.C-R., P.J.M., and S.J.C. contributed to the study conception and design. Material preparation, data collection and analysis were performed by T.D-G., S.P., N.C-R., M.C., E.L.L., C.M, D.H. and J.M. The first draft of the manuscript was written by T.D-G, N.C-R and J.C.K. and all authors commented on following versions of the manuscript. All authors read and approved the final manuscript.

Competing interests
The authors declare no competing interests.

Ethical approval
All applicable international, national, and/or institutional guidelines for the care and use of animals were followed. All procedures performed in studies involving animals were in accordance with the ethical standards of the institution at which the studies were conducted. All experiments and procedures conducted on animals were carried out in accordance with United Kingdom Home Office regulations under the Animal (Scientific Procedures) Act (1986), and were approved by the local ethical review board of the Department of Physiology, Anatomy and Genetics at the University of Oxford.

Additional information
Supplementary Information The online version contains supplementary material available at https://doi.org/10.1038/s41598-025-99580-x.

Correspondence and requests for materials should be addressed to J.C.K.

Reprints and permissions information is available at www.nature.com/reprints.

Publisher's note Springer Nature remains neutral with regard to jurisdictional claims in published maps and institutional affiliations.